MATERIALE PLASTICE
https://revmaterialeplastice.ro
https://doi.org/10.37358/Mat.Plast.1964

Considerations on the Plastic Structure of a UAV Payload Made by 3D Printing Technology

LUCIAN STEFANITA GRIGORE[1*], AMADO-GEORGE STEFAN[2], OCTAVIAN ORBAN[3], IOANA-RALUCA ADOCHIEI[2]

[1]Military Technical Academy Ferdinand I, Faculty of Communications and Electronic Systems for Defense and Security, Department of Electronic Systems and Military Equipment, Center of Excellence in Robotics and Autonomous Systems – CERAS, 39-49 George Cosbuc Av., 050141, Bucharest, Romania
[2]Military Technical Academy Ferdinand I, Faculty of Aircraft and Military Vehicles, Department of Integrated Aviation and Mechanical Systems, 39-49 George Cosbuc Av., 050141, Bucharest, Romania
[3]Military Technical Academy Ferdinand I, Faculty of Integrated Weapons, Genius and Mechatronics Systems, Department of Construction, Genetic Engineering and Geomatics Military Technical Academy Ferdinand I, 39-49 George Cosbuc Av., 050141, Bucharest, Romania

Abstract: *With the development of unmanned aerial vehicle (UAV) systems for a multitude of real-time applications, 3D printing technologies have been developed to make thermoplastic structures by fusing filament Fused Deposition Modeling (FDM) or Fused Filament Fabrication (FFF). However, we consider that the realization of new technologies of experimental models / technological demonstrators / prototypes becomes profitable by using 3D printing technologies. The main aim of the paper is to highlight how the use of three types of materials, which are processed differently, influences the Von Mises stresses of the payload used for a UAV, with the mission of photographing and filming from high altitude.*

Keywords*: Payload, plastic material, 3D printing, PET-G, Textolite, FEM, FEA, own modes of vibration, Natural Frequency, UAV*

1. Introduction

UAVs (Unmanned Aerial Vehicles) [1] are defined as generic air vehicles capable of operating autonomously, without a pilot on board [2]. The most common types of UAVs are multi-rotor, fixed-wing, flap-wing, and hybrid wing systems [2] (Figure1). They are considered very useful for activities such as mapping, topography, telecommunications [3,4], surveillance, and agricultural management [5,6]. The development of technologies for the listed applications was based on innovations in structural and aerodynamic projects. Within the CERAS research center, payloads are designed and made for aerial drones, in order to develop collaborative robotic systems [7-11]. The need for this study is due to increasingly restrictive conditions for reducing carbon emissions [12,13]. Through the introduction of new lightweight materials and manufacturing technologies to enable the development of detection and control systems - payloads [14]. In other words, the use of additive manufacturing allows remote work, and the production of parts, close to the final requirements, consistently reduce emissions due to transport and delivery of parts to a desired location [15-17] (Figure 1).

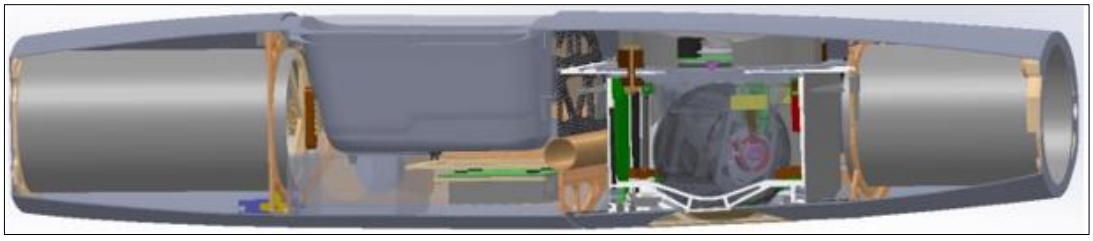

Figure 1. Hirrus 3D model of the drone and the paylaod components [9]

**email: lucian.grigore64@gmail.com*

The payload under discussion equips a fixed-wing UAVs, defined as "air vehicle" which uses fixed wings in combination with forward traction to generate lift [18,19]. Fixed-wing UAVs allow long flights and a degree of operability at high altitudes, as it can carry electronic equipment such as cameras and sensors [20-22].

This study presents the effects of using two materials, one thermoplastic and one rigid. The design and realization of the payload was performed simultaneously with the realization of the UAVS drone - HIRRUS-V1. According to the technical specifications [23,24] the project was carried out on two modules: the air vehicle and the Payload module. SolidWorks software was used for the design, and CFD (Computational Fluid Dynamics) was used for the aerodynamics analysis. Following the analysis of the aerodynamic effects on the UAV structure, the materials for the Figure 1 aircraft were selected. Depending on the subsequent tests, the materials were selected for payload.

One of the materials is the Textolite (Phenolic cotton cloth laminate HGW 2082.5 acc. To DIN 7735) [25] and for the realization of the final products it was subjected to turning, milling, polishing operations and most joints required the insertion of additional elements. It also has a certain degree of nonlinearity when loading / unloading, the stiffness increasing slightly [26]. The layers of the composite material are distributed and oriented according to unidirectional orientations. The inclination of the fibers can be 0°, 45° and 90° to increase the strength of the material [27]. Textolite semi-finished products are subjected to mechanical processing processes, such as: turning, milling, polishing, polishing [28,29]. As a result of these operations, the alignment of the cotton fibers was interrupted and / or delamination was produced in the processing area. All these things can lead to the decrease of the thermomechanical characteristics and also to the modification of the values of the own modes of vibrations [30,31].

The second material is PET-G (Polyethylene Terephthalate - Glycol), which is deposited layer by layer. Other characteristics of PETG can be found in [32] (Table 1, Figure 5).

The third material used is ABS (Acrylonitrile-butadiene-styrene). The material is easy to process without the need for a heated bed and does not produce smoke during construction [33-36].

The analytical models, from the paper, regarding the distribution of efforts in the components of a payload started from the models used for ABS [37].

2. Materials and methods

2.1. Details on numerical modeling of Textolite structures - Phenolic Cotton Cloth Laminate

Textolite is a laminate based on cotton fabric and phenolic resin. This type of material has a high wear resistance because the layers of phenolic resin and those of cotton fabric can be aligned continuously or discontinuously, unidirectional, or bidirectional, in the form of a matrix. Once the Textolite reaches the threshold of the plasticity area, it will suffer a rupture of the cotton fibers, the piece showing traces of exfoliation.

$$E_1 = V_f \cdot E_f + \left(1 - V_f\right) \cdot E_m, \tag{1}$$

where: E_f și E_m - represents the modulus of elasticity of the fiber and the matrix for the range of relevant sections, respectively V_f is the volume fraction of the fiber.

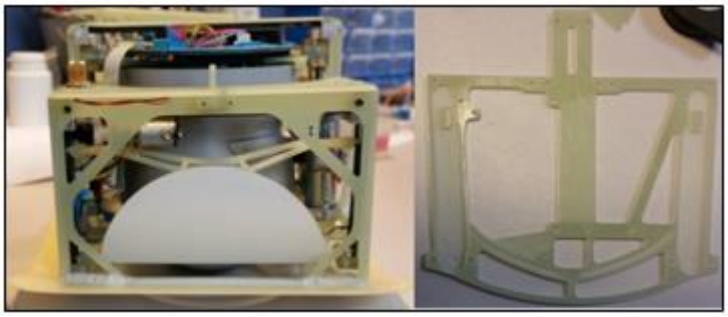

Figure 2. Payload made from textolite

As can be inferred, the critical breaking point of the adjacent fibers triggers the rupture of the pieces in the Textolite. The formation of such a cluster of adjacent fibers depends on the statistical distribution of fiber strengths and the transfer of local stresses in the vicinity of the breaking fibers. This cluster is influenced by the fiber-matrix interface.

The Textolite laminate is quasi-isotropic in nature, so that any crack can be highlighted immediately. For numerical modeling both cotton fibers and laminate are elastic and linear isotropic. The interface between cotton fibers and laminated resin was modeled with a linear softening law with equal critical energy (case of the law of elastic-plastic softening interface).

The component elements of the payload structure made of Textolite come from the processing of plate, bar and pipe type semi-finished products (Figure 2). Analytical-numerical modeling of the stress of a thin plate requires solving three-dimensional elasticity systems of differential equations.

2.2. Considerations regarding the characteristics of the numerical modeling of the PET-G structure

PET-G is a co-polyester thermoplastic material that is deposited by the FDM method. The resulting product is characterized by reasonable tensile strength, impact resistance, durability and flexibility.

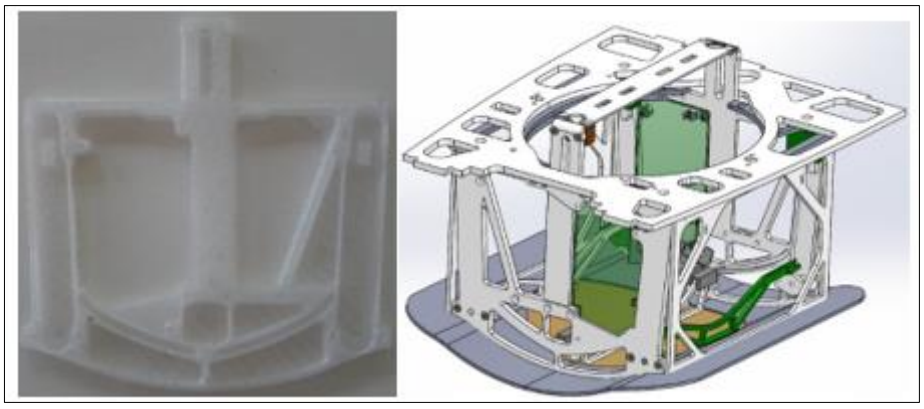

Figure 3. Representation of 3D printed payload elements from PET-G

About PETG it can be appreciated that some elongation of the material can be approximated in terms of tensile stress. On the other hand, it can be seen that it has the characteristics of a material that allows the absorption of a fairly large amount of energy, energy that can generate its own modes of vibration unfavorable on the structure of the payload.

2.3. Numerical modeling when using ABS

Finite element modeling aims to distribute the stresses in the structural parts of the payload made of ABS and test the capacity of the modulus of elasticity by comparing Young's predicted and experimental modulus.

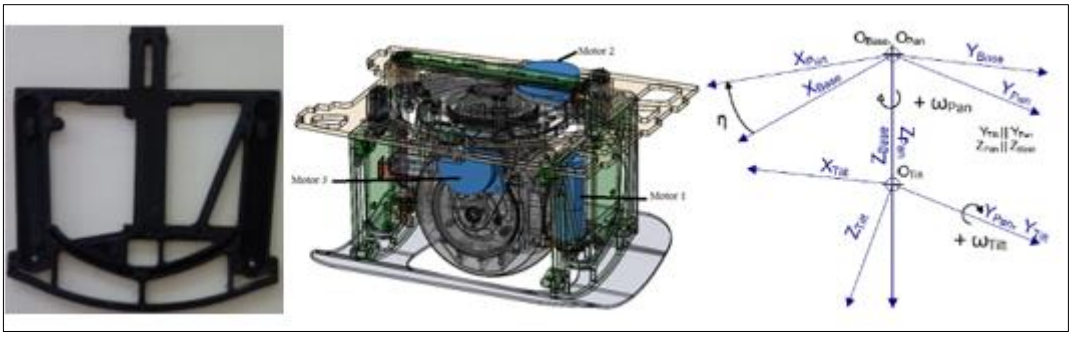

Figure 4. 3D model of the drive components Payload

The geometry is transformed into a finite element mesh in which each element is represented by a cube-type structural element. Each element is defined by eight nodes and each node has three degrees of freedom corresponding to the displacement components (UX, UY, UZ) in the main directions X, Y and Z. The density of the network is adapted according to the degree of approximation of the results to the characteristics provided by the manufacturer.

An ABS with modulus of elasticity of 2 [GPa] and a Poisson's contraction coefficient of 0.394 was used. The simulation of the structure has the following test conditions: the upper end of the structure (the one that does not leave the resting place in the drone during the retraction); and the end provided with hinged doors through which the EO / IR (Electro-Optical / Infra-Red) filming module exits is free in the Z direction.

3. Results and discussions

3.1 Kinematic and dynamic analysis of the Payload compartment door opening

The door has a parallel plane motion, the motion plane being yOz. Figure 5 and Figure 6 show two views of it. In Figure 6 the dimensions corresponding to the kinematic model shown in Figure 7 are highlighted.

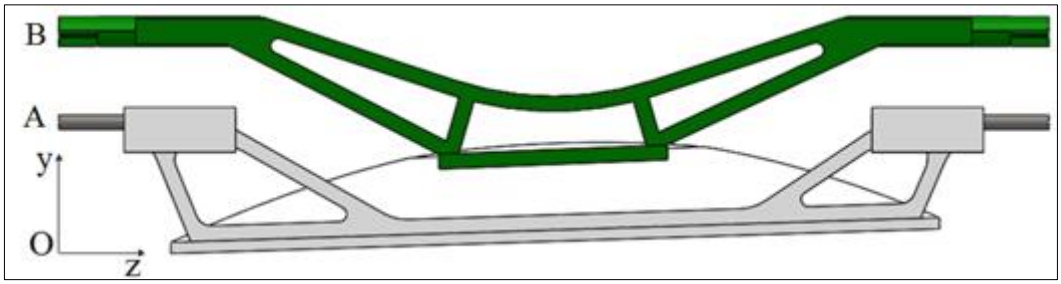

Figure 5. Side view of the payload compartment door assembly

In point "A" is a steel shaft that rests in a curved seat that can slide along it, in point B there is a geometric configuration that allows this end to hang on the side of a closed toothed belt, mounted between two belt wheels.

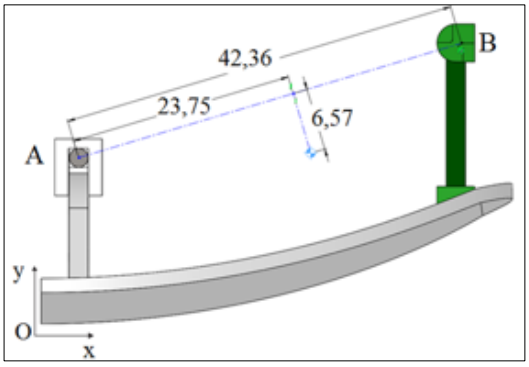

Figure 6. Front view of the payload compartment door assembly

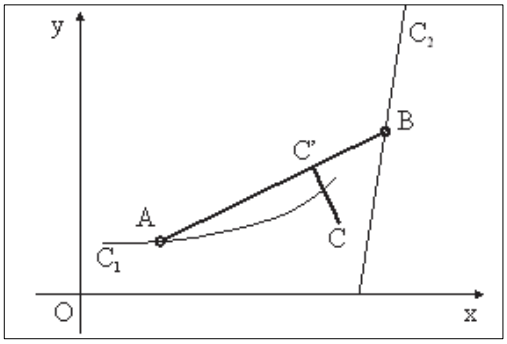

Figure 7. Schematic used in determining the kinematics and dynamic model of the payload compartment door opening

In (Figure 7) point A rests on the curve of the seat (C1) and B rests on the belt, which being stretched and undeformable during movement, represents a linear support (inclined line C2). Point C represents the center of mass and C 'is the projection of the center of mass on the segment AB (Figure 8).

Curve C1 is given by the explicit form:

$$f(x)=311,951\cdot x^2-10,658\cdot x^2+0,396\cdot x+5,28\cdot 10^{-3}, \quad (2)$$

and the line C2 intersects the axis Ox in: $x=42.493[\text{mm}]$, having a slope: $m_{curea}=13.116$. A simple calculation result: $n_{curea}=-0,557$.

The weight of the payload compartment door assembly is: 58.91 [g], and the volume is; 26716.58 [mm^3]. The calculated principal moments of inertia with respect to the central principal system are: $J_1=109026.89\left[g\cdot mm^2\right]$, $J_2=87537.99\left[g\cdot mm^2\right]$ and $J_3=29685\left[g\cdot mm^2\right]$, respectively with respect to the three axes of the reference system.

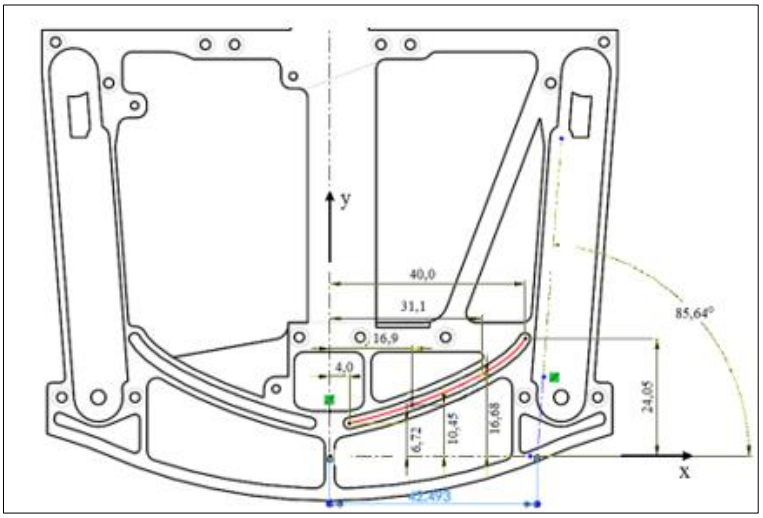

Figure 8. The support plate, made of ABS, with the curved seat and that of the belt system

The moments of inertia with respect to the system originating in the center of mass, with the axes parallel to the axes of the global system are:

$$J_{xx}=29742.82\left[g\cdot mm^2\right];\ J_{xy}=-998.59\left[g\cdot mm^2\right];\ J_{xz}=-1516.41\left[g\cdot mm^2\right],$$
$$J_{yx}=-998.59\left[g\cdot mm^2\right];\ J_{yy}=104427.67\left[g\cdot mm^2\right];\ J_{yz}=8827.89\left[g\cdot mm^2\right],$$
$$J_{zx}=-1516.41\left[g\cdot mm^2\right];\ J_{zy}=8827.89\left[g\cdot mm^2\right];\ J_{zz}=92080.33\left[g\cdot mm^2\right].$$

3.2 Determining the kinematics

A displacement of point B is imposed along the direction of the belt, which depends on the speed of the belt. This law is considered:

$$v(t)=\begin{cases}\dfrac{v_0}{t_0}\cdot t\left[m/s\right], \text{if } t\le t_0\\ v_0\left[m/s\right], \text{if } (t>t_0)\text{and}\, t\le(t_f-t_0)\\ -\dfrac{v_0}{t_0}\cdot t+\dfrac{v_0}{t_0}\cdot t_f\left[m/s\right], \text{if } t\ge(t_f-t_0)\end{cases}, \quad (3)$$

where: $t_0=0,3[s]$ - accelerating/decelerating time from 0 to V_0; $t_0=4,5[s]$ - final time; $v_0=0,011\left[m/s\right]$ - (Figure 9).

The initial position of the door is "closed", point A having the coordinates (4; 6.72).

Using the length of the segment, determine the initial position of point B with the equations of the 2 support curves, resulting in coordinates (44.06; 20.50). Divide the time interval into “n” intervals, denoted by $D_t = \frac{t_f}{n}[s]$, so that the coordinates of point B will be determined by the relation:

$$\begin{cases} x_{B_{j+1}} = x_{B_j} + \dfrac{v\left(t_{j+1}\right)}{\sqrt{1+m_{curea}^2}} \cdot D_t \left[mm\right] \\ y_{B_{j+1}} = m_{curea} \cdot x_{B_{j+1}} + n_{curea} \left[mm\right] \end{cases}. \tag{4}$$

From (4) result the coordinates of point A, determined with:

$$\left(x_{B_{j+1}} - x_{A_{j+1}}\right)^2 + \left[y_{B_{j+1}} - f\left(x_{A_{j+1}}\right)\right]^2 = L_{AB}^2 \left[mm^2\right], \tag{5}$$

where, Oy coordinate is given by: $y_{A_{j+1}} = f\left(x_{A_{j+1}}\right)$.

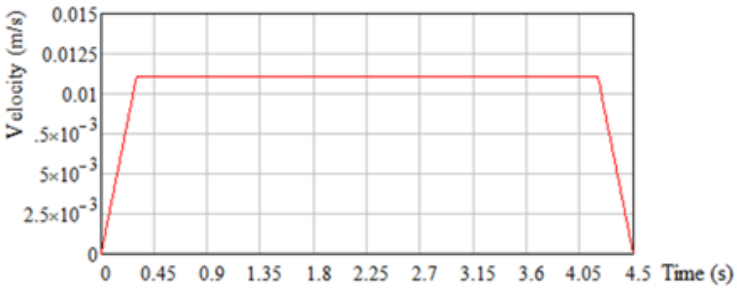

Figure 9. Graphical representation of the speed in point B

It is possible to determine, thus the versor of the oriented vector $\left|\ \overrightarrow{AB}\right.$ and the oriented vector $\left|\ \overrightarrow{AC'}\right.$

$$\begin{cases} \vec{n}_{AB_j} = \dfrac{\left(x_{B_j} - x_{A_j}\right)\vec{i} + \left(y_{B_j} - y_{A_j}\right)\vec{i} + 0\vec{k}}{\sqrt{\left(x_{B_j} - x_{A_j}\right)^2 + \left(y_{B_j} - y_{A_j}\right)^2}} \\ \overrightarrow{AC'}_J = L_{AC'} \cdot \vec{n}_{AB_j} = \left(AC'_x\right)_j \vec{i} + \left(AC'_y\right)_j \vec{j} + 0\vec{k} \end{cases}, \tag{6}$$

because $CC' \perp AB$, direction unit vector of CC' is $\vec{n}_{CC'_j} = \vec{k} \times \vec{n}_{AB_j}$ and $\overrightarrow{CC'_j} = L_{CC'} \cdot \vec{n}_{CC'_j} = \left(CC'_x\right)_j \vec{i} + \left(CC'_y\right)_j \vec{j} + 0\vec{k}$, in which case the coordinates of the point are given by (7) and of the center of mass are given by (8):

$$\begin{cases} x_{C'_j} = \left(AC'_x\right)_j + x_{A_j} \\ y_{C'_j} = \left(AC'_y\right)_j + y_{A_j} \end{cases}, \tag{7}$$

$$\begin{cases} x_{C_j} = -\left(CC'_x\right)_j + x_{C'_j} \\ y_{C_j} = -\left(CC'_y\right)_j + y_{C'_j} \end{cases}, \tag{8}$$

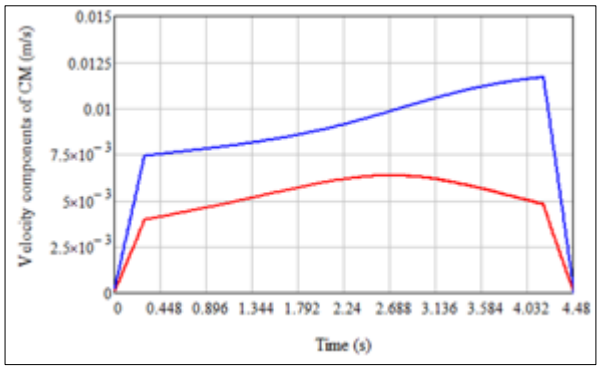

Figure 10. Time variations of the center of mass velocity components

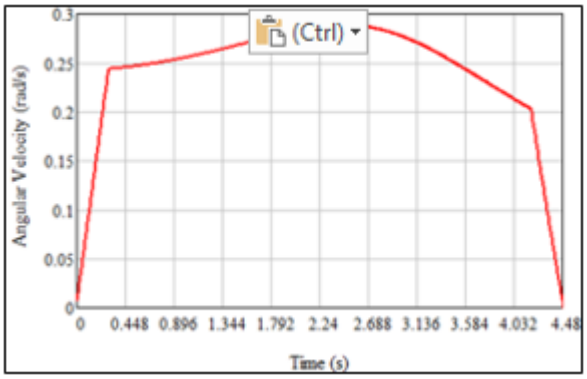

Figure 11. The time variation of the angular speed of the door

The positions of the points in time allow the determination of speeds and accelerations. Thus, the speed and acceleration components of the center of mass (Figure 10) are given by:

$$\begin{cases} v_{C_{x_j}} = \dfrac{x_{C_{j+1}} - x_{C_j}}{D_t} \\ v_{C_{y_j}} = \dfrac{y_{C_{j+1}} - y_{C_j}}{D_t} \end{cases} \dots \begin{cases} a_{C_{x_j}} = \dfrac{v_{C_{x_{j+1}}} - v_{C_{x_j}}}{D_t} \\ a_{C_{y_j}} = \dfrac{v_{C_{y_{j+1}}} - v_{C_{y_j}}}{D_t} \end{cases}, \tag{9}$$

The time variation of the angle of inclination of the segment AB, represents the angular velocity (Figure 11) of the door assembly of the payload compartment.

$$\begin{cases} \omega_j = \dfrac{\operatorname{arctg}\left(\dfrac{y_{B_{j+1}} - y_{A_{j+1}}}{x_{B_{j+1}} - x_{A_{j+1}}}\right) - \operatorname{arctg}\left(\dfrac{y_{B_j} - y_{A_j}}{x_{B_j} - x_{A_j}}\right)}{D_t} \\ \varepsilon_j = \dfrac{\omega_{j+1} - \omega_j}{D_t} \end{cases}, \tag{10}$$

3.3 Dynamic analysis

By isolating the payload compartment door assembly, in point B having a joint and in point A having a simple friction bearing, the situation is obtained from (Figure 12). In what follows, apart from the force of gravity, the terms are dependent on indices j, so, for simplicity, this index is omitted: $\vec{G} = 0\vec{i} - mg\vec{j} + 0\vec{k}$, $\vec{V} = 0\vec{i} + V\vec{j} + 0\vec{k}$, $\vec{H} = H\vec{i} + 0\vec{j} + 0\vec{k}$, $\vec{N} = \lambda \cdot \left(f'_A\vec{i} - 1\vec{j} + 0\vec{k}\right)$, $\left|\vec{N}\right| = \lambda \cdot \sqrt{1 + f'^2_A}$, $\vec{F}_f = -\mu \cdot |\lambda| \cdot \sqrt{1 + f'^2_A} \cdot \left(\dfrac{v_{A_x}}{v_A}\vec{i} + \dfrac{v_{A_y}}{v_A}\vec{j} + 0\vec{k}\right)$, $\left|\vec{F}_f\right| = -\mu \cdot |\lambda| \cdot \sqrt{1 + f'^2_A}$.

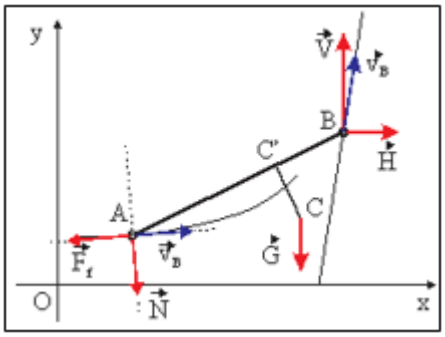

Figure 12. Insulation of the payload compartment door assembly

It follows from the impulse theorem:

$$\begin{cases} m\cdot a_{C_x} = H + N_x + F_{f_x} \\ m\cdot a_{C_y} = V - G + N_y + F_{f_y} \end{cases}, \tag{11}$$

and the kinetic moment theorem written with respect to the center of mass and projected on the Oz axis, results:

$$J_z\cdot\varepsilon = M_C\left(\vec{V}\right)_z + M_C\left(\vec{H}\right)_z + M_C\left(\vec{N}\right)_z + M_C\left(\vec{F}_f\right)_z \tag{12}$$

The following system of equations results from the expressions of forces and relations (11), (12):

$$m\cdot a_{C_x} = H + \lambda\cdot f_A' - \mu\cdot|\lambda|\cdot\sqrt{1+f_A'^2}\cdot\frac{v_{A_x}}{v_A}$$

$$m\cdot a_{C_y} = V - \lambda - \mu\cdot|\lambda|\cdot\sqrt{1+f_A'^2}\cdot\frac{v_{A_y}}{v_A} - m\cdot g$$

$$J_z\cdot\varepsilon = -H\cdot(y_B-y_C) + V\cdot(x_B-x_C) - \lambda\cdot\left[(x_A-x_C)+f_A'\cdot(y_A-y_C)\right] - \mu\cdot|\lambda|\cdot\sqrt{1+f_A'^2}\cdot\frac{v_{A_y}\cdot(x_A-x_C)-v_{Ax}\cdot(y_A-y_C)}{v_A}$$

The system contains three unknown functions: $H(t)$, $V(t)$, $\lambda(t)$. From the first two relations it is determined $H(t)$ and respectively $V(t)$, which are introduced in the last equation, whence its expression results $\lambda(t)$:

$$\lambda = \frac{J_z\cdot\varepsilon + m\cdot a_{C_x}\cdot(y_B-y_C) - m\cdot a_{Cy}\cdot(x_B-x_C) - m\cdot g\cdot(x_B-x_C)}{x_B-x_A+f_A'\cdot(y_B-y_A)-\mu\cdot\frac{|\lambda|}{\lambda}\cdot\sqrt{1+f_A'^2}\cdot\left[\frac{v_{A_x}}{v_A}\cdot(y_B-y_A)+\frac{v_{A_y}}{v_A}\cdot(x_A+x_B-2x_C)\right]}$$

hence the components of the normal reaction force (Figure 13).

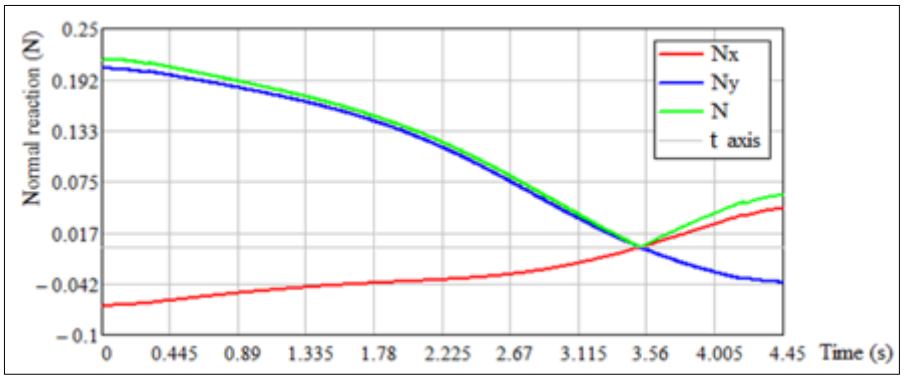

Figure 13. The variation in time of the normal reaction

3.4 Finite element model

In the finite element model a double symmetry of the (Figure 14) structure is considered.

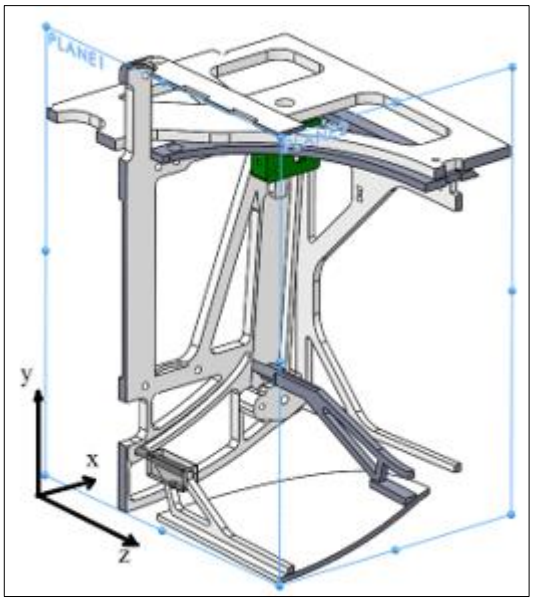

Figure 14. The part of geometry considered

For plane 1 of symmetry, the boundary conditions are displacements along the zero axis Ox, and for plane 2, displacements along the zero axis OZ. It is observed that the maximum normal reaction force is obtained if the payload compartment door is closed, so at the beginning of the opening movement.

All nodes in the mounting holes of the rest of the drone structure have all zero displacements. The nodes in the contact area of the door with the drive belt are also locked. On the steel bolt entering the curved seat, mechanically equivalent forces are distributed with the values of the normal reaction corresponding to the initial moment. The component parts of the considered structure are made of ABS with longitudinal modulus of elasticity, tensile breaking stress, Poisson's ratio 0.394.

The structure was divided with tetrahedral elements. Figure 15 shows the division with elements and a detail of the contact area.

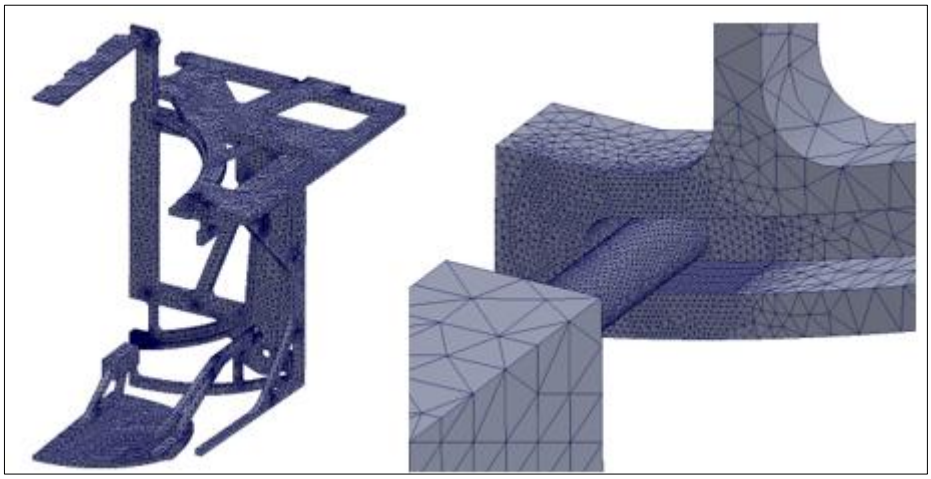

Figure 15. Meshing with tetrahedral elements. Detail of the mesh in the contact area

In (Figure 16) is presented the field of total deformations and in (Figure 17) the field of equivalent stresses in the contact area between the steel bolt and the curved seat of the ABS structure.

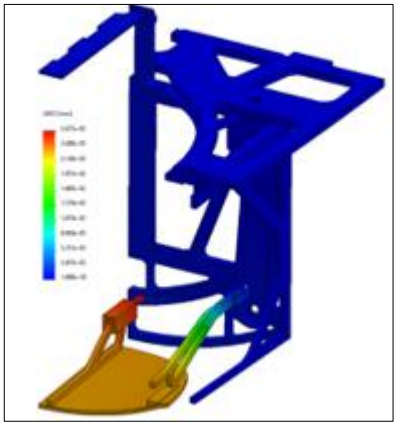

Figure 16. The resulting displacement field

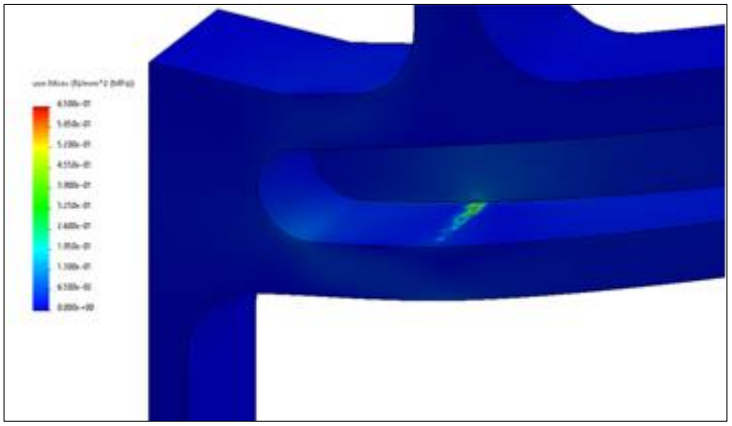

Figure 17. Contact area detail for ABS parts: representation of Von Mises equivalent stresses

4. Conclusions

ABS have some advantages over Textolite and PET-G: greater resistance to thermal degradation; greater thermal stability; a lower statistical dispersion of ABS compared to PET-G; increased flexibility in 3D printing.

It is found that the stresses in the contact area do not exceed 1Mpa, thus being rational the use of plastics in the realization of the component parts of this assembly.

For the future, the action of aerodynamic forces that produce an increase in mechanical stresses must also be considered. Wear will be studied at the contact between two parts, one movable and the other fixed, which slides, and the movement is in the form of cycles. In particular, the traces left will be studied. When paying, the doors have metal elements that lead to bearing wear. A device will be built to simulate a number of movements of the metal elements on different plastics.

Acknowledgments: Thanks to the Military Technical Academy, Center of Excellence in Robotics and Autonomous Systems – CERAS, for making the project data avaible: „*ERL Emergency project: UGV and ROUV*”. We also thank the team members of the ROUV implementation: MOLDER, C., GORGOTEANU, D., CONSTANTIN, D., ȘTEFAN A., MOLDER (MILĂȘAN) A., STOICA, P., FOCȘA, A., and all. Another project for which we thank Military Technical Academy, Center of Excellence in Robotics and Autonomous Systems - CERAS, for making data avaible is „*Manufacturing specification for the product: Protective visor kit RC3/M2 – S.F.1*”, Nr. A3234/2020. We also thank the team members: MOLDER, C., CONSTANTIN, D., GORGOTEANU, D., MOLDER (MILĂȘAN) A., FOCȘA, A., STOICA, P., ANDREESCU, E. The work received support material and scientific advice through the project entitled „ Mini UAVP-06 Autonomous Aerial System” cod SMIS: 50132, agreement Team Net International, division AFT - Autonomous Flight Technologies.

References

1.MOLDER, C., GORGOTEANU, D., CONSTANTIN, D., and all, „ERL Emergency project: UGV and ROUV”, Military Technical Academy, Center of Excellence in Robotics and Autonomous Systems – CERAS, 2019-2021, https://ceras.mta.ro/.

2. HELGE, K., ALEJANDRO DIAZ DE CERIO, S., HANY, H., YAHYA, Z., LAKMAL, S., „Fused deposition modelling for unmanned aerial vehicles (UAVs): A review”, Advanced Engineering Materials, vol. 20, issue 2, 1700552. ISSN (print) 1438-1656, September 2017, http://dx.doi.org/10.1002/adem.201700552.

3.STOICA, P.M., MOLDER, C., "Comparative analysis of methods to detect radio-controlled commercial UAVs.", 4th International Scientific Conference SEA-CONF, 2018 Scientific Bulletin of Naval Academy 2018, Vol. XXI 2018, pg.45-49, https://doi.org/10.21279/1454-864X-18-I1-006.
4.TOMA, Ș.A., SEBACHER, B., FOCȘA, A., "On Anomalous Deformation Profile Detection Through Supervised and Unsupervised Machine Learning.", July 2019 IEEE International Geoscience and Remote Sensing Symposium, https://doi.org/10.1109/IGARSS.2019.8898459.
5.HUANG, S.H., LIU, P., MOKASDAR, A., HOU, L., „Additive manufacturing and its societal impact: a literature review", International Journal of Advanced Manufacturing Technology, vol. 67, pp.1191–1203, July 2013, https://doi.org/10.1007/s00170-012-4558-5.
6.ROMEO, G., FRULLA, G., „Design of High altitude Very-long Endurance Solar Powered Platform for Telecommunication and Earth Observation Applications", Proceedings of DASIA 2002, 13 - 16 May 2002, Dublin, Ireland. Ed.: R. A. Harris. ESA SP-509, Noordwijk, Netherlands: ESA Publications Division, id. 54.1 - 54.12, July 2002, Bibcode: 2002ESASP.509E.54R.
7.BAMBERGER Jr., R.J., WATSON, D.P., SCHEIDT, D.H., MOORE, K.L., „Flight Demonstrations of unmanned Aerial Vehicle swarming concepts", Johns Hopkins Applied Physics Laboratory. Technical Digest, vol. 27, issue 1, 2006.
8.BUGAJSKI, G.T., BS Lieutenant, USAF, „Architectural Considerations for Single Operator management of Multiple Unmanned Aerial Vehicles", Theses and Dissertations, AFIT/GSE/ENV/10-M03, 17 June 2010.
9.PATRICIU, V., PRIESCU, I., NICOLAESCU, S., "Operational Security Metrics for Large Networks.", Volume: I (2006), No: Suppl. Issue, International Journal of Computers, Comm&Control (IJCCC) 2006, Oradea, pg 349-354, ISSN 1841- 9836; E-ISSN 1841-9844, 2006.
10.LIU, Z.C., JIANG, Q., M.L., Yu, H., Woods, B.K.S., „Sustainability of 3D Printing: A Critical Review and Recommendations", Proceeding Conference: ASME 2016, At: Blacksburg, Virginia, USA, Volume: Materials; June 2016, https://doi.org/10.1115/MSEC2016-8618.
11.GORGOTEANU, D., MOLDER, C., "Electric powered miniature vehicle for multi-agent network testbed.", Electric Vehicles International Conference, EV2019, 3-4 October 201, Bucharest, 978-1-7281-0791-2/19/$31.00 ©2019 IEEE, https://doi.org/10.1109/EV.2019.8892953.
12.FALUDI, J., YIU, F., SROUR, O., KAMAREDDINE, R., ALI, O., MECANNA, S. „Do Student Trials Predict What Professionals Value in Sustainable Design Practices?", ASME, Journal of Mechanical Design, vol. 141, issue 10, 102001, October 2019.
13.ROMEO, G., FRULLA, G., CESTINO, E., „Design of a High-Altitude Long-Endurance Solar-Powered Unmanned Air Vehicle for Multi-Payload and Operations", Proceedings: Journal of Aerospace Engineering, vol. 221, issue 2, pp. 199-216, 1 February 2007.
14.FALUDI, J., Van SICE, C., SHI, Y., BOWER, J., BROOKS, O., „Novel Materials Can Radically Improve Whole-System Environmental Impacts of Additive Manufacturing", Journal of Cleaner Production, 212, pp.1580-1590, 1 March 2019.
15.FALUDI, J., GILBERT, C., „Best practices for teaching green invention: Interviews on design, engineering, and business education.", Journal of Cleaner Production, 234, pp.1246-1261, 10 October 2019, https://doi.org/10.1016/j.jclepro.2019.06.246.
16.FALUDI, J., ALI, O., SROUR, O., MECANNA, S., KAMAREDDINE, R., CHATTY, T., „Preliminary Results Testing What Different Design Solutions Arise from Different Sustainable Design Methods", Proceedings, vol. 1, issue 1, pp. 3351-3360, Cambridge University Press, 26 July 2019, https://doi.org/10.1017/dsi.2019.342.
17.***Proiect POS-CCE 2007-2013, Autonomous mini-UAV aerial system. ROBONET financed by the Sectoral Operational Program "Increasing Economic Competitiveness (POS CCE) 2007-2013" - Cod SMIS 50132- S.C. EN-GENIUS SOLUTIONS S.R.L.
18.CUSTERS, B., „The Future of Drone Use: Opportunities and Threats from Ethical and Legal Perspectives", T.M.C. Asser Press Springer, 2016, ISBN 978-94-6265-131-9, ISSN 1570-2782, https://doi.org/10.1007/978-94-6265-132-6.

19.FARRELL, J.A., „Aided Navigation. GPS with High Rate Sensors.", Editor Department of Electrical and Computer Engineering. Riverside: The McGraw-Hill Companies, Inc. Accesat 10 10, 2018, https://doi.org/10.1036/0071493298.
20.GREWAL, M.S., ANDREWS, A.P., BARTONE, C.G., „Global Navigation Satellite Systems, Inertial Navigation, and Integration." 3rd Edition. Nw York, New York: John Wiley & Sons, February 2013.
21.LAZLO, T., WOOLSEY, C.A., MORGANSEN, K.A.,. „Planar Path Planning for Flight Vehicles in Wind with Turn Rate and Acceleration Bounds." 2010 IEEE 3240-3245, May, 3-7, 2010 https://doi.org/10.1109/ROBOT.2010.5509862.
22.ABBA, G., ABDERRAHIM, M., et all., „Unmanned Vehicles (UV) for Aerial, Ground and Naval Military Operations.", RTO-MP-052, NATO RTO Report (Unclassified), 1 January 2002, https://doi.org/10.14339/RTO-MP-052.
23.NGUYEN, H.G., BOTT, J.P., „Robotics for law enforcement: Applications beyond explosive ordnance disposal", Proceedings of SPIE - The International Society for Optical Engineering, vol. 4232, Enabling Technologies for Law Enforcement and Security, 21 February 2001.
24.CORIGLIANO, A., „Comprehensive Structural Integrity. Volume 3: Numerical and Computational Methods, chapter 3.09 - Damage and Fracture Mechanics Techniques for Composite Structures, subchapter 3.09.7.4.4", pp. 459-539, ISBN: 978-0-08-043749-1, 2003, https://doi.org/10.1016/B0-08-043749-4/03041-X.
25.SMITH, P.A., „Comprehensive Composite Material. Volume 2: Polymer Matrix Composites, chapter 2.04 - Damage and Fracture Mechanics Techniques for Composite Structures, subchapter 2.04.4.2", pp. 107-150, ISBN: 978-0-08-042993-9, 2000.
26.LAMB, J.J., ALBRECHT, I., AXILROD, B.M., „Mechanical Properties of Laminated Plastics at -70^0, 77^0, and 200^0 F", U. S. Department of Commerce National Bureau of Standards, Research Paper RP2028 Volume 43, September 1949, Part of the Journal of Research of the National Bureau of Standards, Technical Notes 1054 and 1550.
27.HOCHENGA, H., TSAO, C.C., „Effects of special drill bits on drilling-induced delamination of composite materials.", International Journal of Machine Tools & Manufacture, vol. 46, pp. 1403–1416, 2006, https://doi.org/10.1016/j.ijmachtools.2005.10.004.
28.S. R. PATEL, S.R., „A study on delamination of cotton fibre reinforced phenolic resin composite material due to drilling", ResearchGate, June 2010, https://www.researchgate.net/publication/325711191
29.BARAN, I., TUTUM, C.C., NIELSEN, M.W., HATTEL, J.H., „Process induced residual stresses and distortions in pultrusion", Composites Part B: Engineering, ISSN: 1359-8368, vol. 51, August 2013, pp. 148-161, https://doi.org/10.1016/j.compositesb.2013.03.031.
30.CHOUDHARY, T., KUMAR, A., „Vibration Analysis of Stiff Plate with cut-out", International Journal of Technical Research and Applications, e-ISSN: 2320-8163, www.ijtra.com, vol. 3, issue 1, pp. 135-140, Jan-Feb 2015, https://www.ijtra.com/ijtra-issue151.php.
31.GUESSASMA. S., BELHABIB, S., NOURI, H., „Printability and Tensile Performance of 3D Printed Polyethylene Terephthalate Glycol Using Fused Deposition Modelling", MDPI, Polymers, vol. 11, issue 7, no. 1220, pp.16, 22 July 2019, https://doi.org/10.3390/polym11071220.
32.BLOK, L.G., LONGANA, M.L., Yu, H., Woods, B.K.S., „An investigation into 3D printing of fibre reinforced thermoplastic composites", Additive Manufacturing, vol. 22, pp. 176–186, Aug. 2018, https://doi.org/10.1016/j.addma.2018.04.039.
33.ADAM, G.A.O., D. ZIMMER, D., „Design for Additive Manufacturing Element Transitions and Aggregated Structures.", CIRP Journal of Manufacturing Science and Technology, vol. 7, pp. 20-28, 2014, https://doi.org/10.1016/j.cirpj.2013.10.001.
34.ROTARIU, A., BUCUR, F., TOADER, G., LUPOAE, M., SAVA, A.C., SOMOIAG, P., CIRMACI MATEI, M., "Experimental Study on Polyurea Coating Effects on Deformation of Metallic Plates Subjected to Air Blast Loads", *Mater. Plast.*, **53**(4), 2016.

35.BARZIC, A.I., ALBU, R.M., NECHIFOR, C.D., POSTOLACHE, M., LOGIGAN, C., DOROHOI, D.O., "Surface Processing of Polyethylene Terephthalate for Orientation of Nematics in Display Devices", *Mater. Plast.*, **57**(2), 2020, 1-7.
36.IFTIMIE, B., LUPOAE, M., ORBAN, O., "Experimental Investigations Regarding the Behaviour of Composite Panels Based on Polyurea and Kevlar or Dyneema Layers Under Blast and Fragments.", *Mater. Plast.*, **56**(3), 2019, 538-542.
37.DRAGHICI, S., VINTILA, I.S., MIHALACHE, R., PETRESCU, H.A., TUTA, C.S., HADAR, A., "Design and Fabrication of Thermoplastic Moulds for Manufacturing CFRP Composite Impeller Blades", *Mater. Plast.*, **57**(1), 2020, 290-298.

Manuscript received: 14.07.2020